
Article:
Hamdi, N., Hidaoui, S., Hassani, H.O. et al. (4 more authors) (2020) Synthesis, crystal structure, physical and catalytic oxidation studies of a new hybrid phosphate [(N2H5)2Co(HPO4)2]. Journal of Molecular Structure, 1217. 128317. ISSN 0022-2860

https://doi.org/10.1016/j.molstruc.2020.128317

Synthesis, crystal structure, physical and catalytic oxidation studies of a new hybrid phosphate [$(N_2H_5)_2Co(HPO_4)_2$]

Najlaa Hamdi[1], Safaa Hidaoui[1], Hicham Oudghiri Hassani[1], Mohammed Lachkar[1], Michal Dusek[2], Nicola Morley[3] and Brahim El Bali [4,*]

[1] Engineering Laboratory of Organometallic and Molecular Materials, Faculty of Sciences, University Sidi Mohamed Ben Abdellah, Po. Box 1796 (Atlas), 30000 Fez, Morocco

[2] Institute of Physics of the Czech Academy of Sciences, Na Slovance 2, 182 21 Praha 8, Czech Republic.

[3] Royal Society Leverhulme Trust Senior Research Fellow 2018-2019

Department of Materials Science and Engineering, University of Sheffield, Sheffield S1 3JD, United Kindgdom

[4] Independent scientists; Email: b_elbali@yahoo.com

Abstract

A new one-dimensional coordination polymer [$(N_2H_5)_2Co(HPO_4)_2$] was synthesized by slow evaporation method and characterized by means of single-crystal X-ray diffraction, Fourier Transform Infrared Spectroscopy (FTIR) and Thermogravimetric Analysis (TGA). Its catalytic activity was tested using UV-visible absorption measurements. The compound crystallizes in the monoclinic system (S.G: $P2_1/c$) with the cell parameters (Å, °): a= 5.3665(3), b= 11.1271(6), c= 7.7017(4), β= 104.843(4), V= 444.55(4) $Å^3$ and Z= 2. The crystal structure, consisting of a linear chain, is made of rings of [CoN_2O_4] octahedra and [$PO_3(OH)$] tetrahedra sharing vertices via oxygen atoms coordinated to cobalt centers. The rings are linked to chains running along [100] and form thereby polymeric chains that are

connected by hydrogen bonds in a three-dimensional arrangement. The FTIR spectroscopy shows the expected bands of hydrazine and phosphate groups. The thermal behavior consists mainly of the loss of hydrazine moieties leading thus to the formation of anhydrous cobalt phosphate. The phosphate complex exhibits efficiency in catalytic oxidation and degradation of methylene blue dye. The ac magnetic susceptibility shows a peak indicating antiferromagnetic order with a Neel temperature of 5.5 K. Fitting the Curie-Weiss equation to the ac magnetic susceptibility above 50 K gives the average Curie-Weiss Constant to be -11.8 K.

Keywords: Cobalt; Crystal structure; Spectroscopy; Catalysis; Magnetism.

I. Introduction

The synthesis of transition metal phosphates has been the focus of much scientific research owing to their interesting electrical, magnetic properties and their conventional applications as absorbents, ion exchangers and catalysts [1-5]. The metal phosphates for the most part exhibit three-dimensional layer structures comparing with those with one-dimensional structures [6-10]. Structures with this dimensionality result either as edge-shared ladders or corner-shared linear chains. The use of organic amines as structure-directing agents or templates in the synthesis of open-framework metal phosphates is well documented [1]. In some metal phosphates, amine molecules either act as ligands and bond via nitrogen to the metal centers to form MO_xN_y units within the framework or by H-bonds. Hence, several metal phosphates containing such units have been prepared using amines molecules [11-16]. Bridging ligands like hydrazine are widely used in coordination polymers and have been found to be very effective in the formation of various interesting extended structures [17]. The self-assembly of these structures leads to the formation of coordination polymers which are an important class

of materials because of their potential application in advanced materials [18]. In this context, we report herein on the synthesis, crystal structure, spectroscopic characterization, thermal behavior and magnetic study of a new Co^{II} one-dimensional coordination polymer. As matter of application, the new hybrid phosphate was tested as a catalyst for the oxidation and degradation of methylene blue (MB) dye with hydrogen peroxide.

II. Experimental

II.1. Crystal synthesis

All reagents were acquired from commercial sources and used without further purification. Single crystals of $[(N_2H_5)_2Co(HPO_4)_2]$ were synthesized under ambient conditions. The reaction mixture was prepared with 20 mL of distilled water, 10 mmol (0.6 mL) of H_3PO_4 acid (85%, M = 98 g/mol) (Prolabo) and 2 mmol (0.48 g) of $CoCl_2.6H_2O$ (Prolabo). To the pink solution, 10 drops of $(NH_2)_2$ (1M) were added, final pH = 5. The mixture was left at room temperature. After three weeks, pink rod-like crystals were collected, washed with distilled water and dried in air.

II.2. infrared spectroscopy analysis and Thermal Analysis

Infrared spectrum of the compound was recorded on a VERTEX 70 FTIR Spectrometer in the range 4000-400 cm^{-1} using the ATR technique at 4 cm^{-1} resolution. Thermogravimetric analysis (TGA) data were recorded on an SDT-Q600 analyzer from TA instruments. The temperature varied from RT to 1000 ºC at a heating rate of 10 ºC·min^{-1}. Measurements were carried out on samples in open platinum crucibles under air flow.

II.3 Magnetization and AC susceptibility Measurements

A MPMS-3 VSM-SQUID magnetometer was used to measure the magnetization and ac susceptibility of the sample as a function of magnetic field and temperature. The magnetization as a function of magnetic field was measured at 2.5 K, 10 K and 300 K. The

magnetization and ac susceptibility were measured as a function of temperature between 2 K and 300 K, with a detailed measurement carried out below 60 K. The sample was cooled down in zero magnetic field, to 2 K, where a DC field of 100 Oe was applied. The magnetization and ac susceptibility were then measured as a function of temperature up to 300 K, this is the zero-field cooled (ZFC) data, the measurement was repeated from 300 K to 2 K for the field cooled (FC) data. The ac susceptibility was measured at 10, 100 and 1000 Hz.

II.4. Catalytic activity

The catalytic efficiency of cobalt phosphate complex was evaluated for the oxidation and degradation of an organic dye by following an experimental protocol as defined previously in literature [**19**]. In a typical experiment, 45 mL of methylene blue (MB) (5 ppm), 5 mL of hydrogen peroxide (30%), and 0.1 g of $(N_2H_5)_2Co(HPO_4)_2$ were mixed and kept under constant magnetic stirring at room temperature. The reaction was followed by ultraviolet-visible (UV-Vis) spectrophotometer.

II.5. Crystal structure determination

II.5.1. Single crystal study

A crystal of dimensions 0.46 × 0.21 × 0.18 mm was selected for X-ray diffraction analysis. Data were collected at room temperature with an Oxford diffraction CCD diffractometer Gemini using graphite-monochromated MoK_α radiation (λ= 0.7173 Å), registered with an Atlas S2 CCD area detector. Data were processed with the program Crysalis RED [20]. The phase problem was solved by direct methods using Superflip [21] and the structure was refined with Jana2000 [22]. The structural graphics were created using DIAMOND program [23]. Data collection and refinement details of $[(N_2H_5)_2Co(HPO_4)_2]$ are reported in Table 1. The atomic coordinates are reported in Table 2, while Table 3 contains the basic geometrical data and hydrogen bonds in Table 4. Hydrogen atoms were kept in an ideal geometry for NH_3

group while for NH_2 and OH their position was refined using bond restraint 0.87 Å for N-H and 0.86 Å for O-H. The temperature parameters of all H atoms were constrained to a 1.2 multiple of the equivalent isotropic temperature parameter of the parent atom. CIF files have been deposited [**CCDC 1836791**], and can be obtained free of charge using the link: www.ccdc.cam.ac.uk or from the CCDC, 12 Union Road Cambridge CB2 1EZ, UK; fax: +44 1223 336033; E-mail: deposit@ccdc.cam.ac.uk].

III. Results and discussion

III.1. Complex identification and characterization

III.1.1. Structural description

The unit cell of $[(N_2H_5)_2Co(HPO_4)_2]$ contains 8 non hydrogen atoms with the crystallographically distinct Wyckoff site 2a for Co^{2+} (Fig. 1). As shown in Fig.2, Co atom lies thus in an octahedral coordination made of four adjacent O atoms belonging each the symmetry-related $PO_3(OH)$ tetrahedrons forming the base, while two N atoms, from two symmetrical hydrazinium ions, site on the remaining trans apices of the octahedron. The Co–O bond lengths are in the range 2.0903(2)-2.1011(17) Å [av. 2.0957 Å] and the Co–N bonds have an average distance of 2.137 Å, which might be compared to 2.093(2) Å reported for $(NH_4)[Co(H_2O)_6]_3(HPO_3)_4$ [24], or 2.092 Å for $(DACH)_{0.5}Co_3(H_2O)(OH)(PO_4)(HPO_4)(3+x)H_2O$ [25]. The square planar arrangement around the Co atom is slightly distorted, with O2–Co–$O2^i$ and O3-Co-$O3^i$ angles both of 180.0(5)° (Table 3). According to the formula $\Delta_{oct} = 1/6*\Sigma[(d_i-d_m)/d_m]^2$ [26, 27], the bond-length distortions for the Co atom amount $32.6\cdot10^{-3}$, which indicates heavy distortion of the Co octahedron as to compare with the value $4.532\cdot10^{-3}$ found in the hybrid hypophosphite $[Co(H_2PO_2)(C_{12}N_4H_{16})]Cl_2$ [28].

The P atom has a tetrahedral connectivity and possesses one terminal P–OH bond. The P–O bonds exhibit a mean value of 1.521 Å for three non-hydroxyl oxygen atoms, and slightly longer bond 1.598(24) Å for the hydroxyl. The hydrazine N_2H_4 molecule is protonated to $N_2H_5^+$ and acts as a monodentate terminal ligand, which is confirmed by the slight short distance between the two nitrogen atoms (1.443 Å). The hydrazinium ions participate in hydrogen bonds towards oxygen atoms of $PO_3(OH)$ anions. There is also a moderate hydrogen bond connecting two symmetry-related $PO_3(OH)$ anions via hydrogen of the hydroxyl. The complex compound of $[(N_2H_5)_2Co(HPO_4)_2]$ might be described in terms of rings of $[CoN_2O_4]$ octahedra and $[PO_3(OH)]$-tetrahedra sharing vertices *via* oxygen atoms coordinated to cobalt. The rings form an infinite chain running along b direction (Figure 3) and give rise to a one-dimensional coordination polymer. The polymeric chains are further connected by hydrogen bonds N-H···O and O-H···O into a three-dimensional extended network (Table 4, Figure 4).

For testing purity of the bulk sample used for the other measurements, we recorded a powder XRD pattern of the grounded crystals of the title compound and compared with simulated diffraction pattern (Fig. 5). The two spectra match well, indicating that the spectroscopic, thermal and magnetic results of $[(N_2H_5)_2Co(HPO_4)_2]$ should be fully correlated with the crystal structure data.

III.1.2. Fourier Transform Infrared Spectroscopy

As shown in Figure 6, the infrared spectrum of the complex compound exhibits bands corresponding to the vibration modes of hydrazine and phosphate moieties. The broad band at 3474 cm^{-1} is due to the stretched vibration of primary amine [29]. The set of bands occur in

the range 3180–3320 cm^{-1} correspond to the asymmetric stretching mode of υ_{as}(N-H), while the absorption located at 2659 cm^{-1} can be assigned as a stretching mode of $\upsilon(NH_3^+)$ in hydrazinium cation [30]. The medium peak observed near to 1612 cm^{-1} corresponds to the bending vibration of $\delta(NH_2)$, whilst the intensities at 1140 cm^{-1} and 1283 cm^{-1} are associated to their twisting and wagging modes respectively [31]. These bands confirm the presence of the hydrazine molecule in its protonated form in the structure [29]. The Absorption frequency centered at 2424 cm^{-1} is due to the combination of phosphate bands [32]. The set of bands appearing in 1140-800 cm^{-1} can be attributed to asymmetric and symmetric stretches of P-O bonds [33], whereas the weak band at 1492 cm^{-1} is assigned to the bending mode of the (PO-H) group [34].

III.1.3. Thermal behavior

In order to examine the thermal stability of $[(N_2H_5)_2Co(HPO_4)_2]$, a TGA experiment was performed under air atmosphere. The experimental analysis (Fig. 7) shows two separated steps of weight loss in a total of 34 %. The weight loss depicted in the temperature region 220-520 °C is attributed to the decomposition of amine molecules and phosphate groups. The first mass loss of 30 % in the range of 200-500 °C is accompanied by an endothermic signal in DTA trace at 240 °C. The sharp peak indicates a vigorous and continuous weight loss which can be attributed to the dehydrazination of the cobalt complex (calculated weight loss 29.3 %). The second stage (observed 4 %) starting at about 520 °C and ending at 560 °C corresponds to the formation of $Co(PO_3)_2$ cobalt phosphate compound. This phenomenon is coupled with a small exothermic curve at 520 °C (calculated weight loss 5 %). To confirm this result, the infrared spectrum depicted on Figure 8 shows the solid residue heated at 600 °C, which reveals characteristic bands corresponding to the vibration modes of the metaphosphate material which has been identifying as $Co(PO_3)_2$.

III.1.4. Oxidation of methylene blue test

The complex compound was tested as a catalyst that degrades the methylene blue dye with hydrogen peroxide under ambient conditions. The variation of methylene blue concentration as a function of time after adding $[(N_2H_5)_2Co(HPO_4)_2]$ catalyst and without a catalyst was measured by a UV-visible absorption spectrophotometer, and presented in Figure 9. After one day of reaction, the concentration of pure methylene blue has not changed. While, the oxidation of the methylene blue by hydrogen peroxide without catalyst has a small advancement of about 4 % in the first contact and stay unchanged during the time.

However, the absorbance at 665 nm corresponding to the methylene blue decreases until 10% and 3 % during 2 hours for 0.1 g and 0.15 g of the cobalt phosphate complex respectively inducing the oxidation of methylene blue. The action of the catalyst was also followed by the change the color of the solution. In fact, a gradual decrease from dark blue to light pink, was observed leading thus to a total discoloration. This result exhibits a good catalytic efficiency of the synthesized compound. In order to complete the catalytic activity, we propose to study the possible reaction mechanism.

It was found that the complete oxidative mineralization of MB by H_2O_2 in the presence of a catalyst produced CO_2, HNO_3, H_2SO_4 and HCl [35]. Therefore, the stoichiometric equation (1) can be written as:

$$C_{16}H_{18}N_3SCl + 52H_2O_2 \xrightarrow{[(N_2H_5)_2Co(HPO_4)_2]} 16CO_2 + 0.5O_2 + 58H_2O + 3HNO_3 + H_2SO_4 + HCl \quad (1)$$

On the other hand, during the oxidation experiment of MB, it is worthwhile to mention that some color change on the surface of the catalyst with the change of the pH of solution. In fact, the pH of the MB solution was 6.5 before the addition of the H_2O_2 and decreased to 4.2 once the H_2O_2 was added. However, the pH increased to 6.35 after the addition of the catalyst accompanied with a color change from light pink to light blue. When the oxidation of the MB

solution was completed (after 2 hours), the pH decreased to 4.95, and the catalyst resumed its native color. On another side, no color change was observed when the $[(N_2H_5)_2Co(HPO_4)_2]$ was mixed either with H_2O_2 or with MB.

Indeed, the formation of the colored intermediate on the surface of the catalyst has an inhibiting effect on the decomposition of H_2O_2. This peroxo-intermediate can attack methylene blue to give methylene blue radical species, MB.OOH$^{\bullet}$, which in turn decomposes to give the reaction products as indicated by the following mechanism:

$$[(N_2H_5)_2Co^{2+}(HPO_4)_2] + H_2O_2 \longrightarrow [(N_2H_5)_2Co^{2+}(HPO_4)_2](OOH) + H^+ \quad (2)$$

peroxo-complex

$$[(N_2H_5)_2Co^{2+}(HPO_4)_2](OOH) + MB \longrightarrow MB(OOH^{\bullet\cdot}) + [(N_2H_5)_2Co^{+}(HPO_4)_2] \quad (3)$$

$$MB(OOH^{\bullet\cdot}) \longrightarrow \text{oxidation products} \quad (4)$$

$$[(N_2H_5)_2Co^{+}(HPO_4)_2] + H_2O_2 \longrightarrow [(N_2H_5)_2Co^{2+}(HPO_4)_2] + 0.5O_2 + H_2O \quad (5)$$

This mechanism is supported by three facts. First, the pH decreases with the progress of the reaction (according to Eq. (2)) having a constant value at the end of the reaction. Second, the reaction can proceed even if the catalyst is removed from the reaction mixture after few minutes from the start of the reaction. This confirms the formation of highly reactive species in the aqueous solution, which might be MB.OOH$^{\bullet}$ radicals according to Eq. (3). Thirdly, the color change from light pink to light blue during the reaction confirms that the cobalt was the catalytic site of activation and changes its oxidation degree from +2 to +1 according to Eg.(3). At the end of reaction, the solution is colorless, while the particles of $[(N_2H_5)_2Co(HPO_4)_2]$ resume a light pink color according to Eqs. (4) and (5). Salim and El-Maazawi also proposed the same mechanism during the study of the kinetics and mechanism of color removal of methylene blue with hydrogen peroxide catalyzed by some supported alumina surfaces [35].

III.1.5. Magnetic study

Magnetic measurements were used to determine whether spontaneous magnetization, such as ferromagnetism, ferrimagnetism or antiferromagnetism occurs with the sample. As the shape of the temperature dependence of magnetization $M(H)$ is indicative of the origin of the magnetic properties. However, it is necessary to correlate the magnetic susceptibility χ *vs*(T) curves and isothermal $M(H)$ plots for a complete analysis of the magentic properties of the sample [36].

The magnetisation of the sample was measured as a function of magnetic field and temperature. From Figure 10, the change in magnetisation as a function of temperature is given. From this data at temperatures above 100 K, the Curie constant can be determined, from $M = \frac{CH}{T}$, taking H = 100 Oe. Thus fitting to the data gives C = 2.94 emu.K/G.mol. The inset of Figure 10, gives the M vs H loops at 300 K, 5 K and 2.5 K. At 300 K, the sample is paramagnetic, hence the linear response with field. Using $M = \frac{CH}{T}$, again with this time T = 300 K, gives C = 3.12 emu.K/G.mol. Thus there is good agreement between the measurements. At 2.5 K and 5 K, the sample is antiferromagnetic, thus the M vs H loop shows a linear dependence of the magnetisation with field up to 40 kOe, then above 40 kOe, "saturation" occurs. From equation (2), the effective magnetic moment can be calculated from the measured Curie constant, this gives μ_{eff} = 4.99 μ_B (M-H data, Figure 10 inset) and μ_{eff} = 4.85 μ_B (M-T data, Figure 10).

From the high temperature ac susceptibility data (Figure 11), Curie-Weiss Law given by:

$$\chi = \chi_o + \frac{C}{(T+\theta_{CW})} \qquad \textbf{(1)}$$

Where χ_o is the temperature-independent susceptibility and θ_{cw} is the Curie-Weiss Constant. This equation can either be fitted to the high temperature ac susceptibility data (Figure 11), between 150 K and 300 K or the $T\chi$ verus temperature data (Figure 12). From figure 11, this

gives χ_o = -2.93e^{-4} emu/mol/Oe, θ_{cw} = -12.2 K and C = 3.17 emu.K/G.mol. Thus the Curie constant is in good agreement with those measured from the magnetisation data. If the Curie constant determined from the magnetisation data, 3.12 is used in equation (1) for the fitting of the data, then χ_o = -1.75e^{-4} emu/mol/Oe, and θ_{cw} = -10.5 K. From Figure 12, fitting equation (1) in the temperature range 100 K to 300 K, gives C = 3.11 emu.K/G.mol and θ_{cw} = -12.6 K, again in good agreement with the values calculated using the other data. Therefore an average Curie Constant and Cuire-Weiss constant can be calculated from the three different fitted data sets. This gives the average Curie constant to be 3.09 emu.K/G.mol and the average Curie-Weiss constant to be –11.8 K.

It is also observed from the zero-field cooled data (Figures 10 and 11), that the magnetisation peaks at 5 K and the ac susceptibility (χ') peaks at 5.3 K. From Figure 11 inset, there is no difference in the peak position between the different frequencies measured. From the imaginary ac susceptibility (χ'') (Figure 12 inset), it is observed that χ'' is positive and roughly constant between 300 K and 45 K, before decreasing and becoming negative with a minimum at 5.3 K. Only the 1000 Hz data are shown, as the signal to noise ratio on the 10 Hz and 100 Hz was too small, such that it was not possible to determine the trends, as observed in the 1000 Hz χ'' data.

The effective magnetic moment can be determined using the equation $\mu_{eff} = 2.828\sqrt{T\chi}$, where T is the temperature and χ is the susceptibility thus taking $T\chi$ between 150 K and 300 K from Figure 12 for all three frequencies, μ_{eff} = 4.85 μ_B. This is in excellent agreement with effective magnetic moment determined from the Curie constants above. Previous measurements of Co^{2+} ions gave the mean effective magnetic moment to be 4.8 μ_B, when the Co^{2+} ions are in an isolated high spin state. The measured effective moment for

$[(N_2H_5)_2Co(HPO_4)_2]$ is in good agreement with these previous measurements of Co^{2+} ions, thus they can be taken to be isolated, with the ions in a high spin state.

From theory, the Curie constant is given by:

$$C = \frac{\mu_B^2}{3k_b} n g^2 \big(J(J+1)\big) = \frac{n\mu_{eff}^2}{3k_B} \qquad (2)$$

Where μ_B is the Bohr magnetron, k_B is the Boltzmann constant, n is number of magnetic atoms per unit volume, g is the Lande g-factor, J is the angular momentum quantum number and μ_{eff} is the effective magnetic moment. Thus the effective magnetic moment and the Curie constant can be calculated for the sample, for $n = 1$, and assuming $g = 2$ and $J = 3/2$ with the Co ions being in a 2+ state. This gives $C = 1.87$ emu.K/G.mol and $\mu_{eff} = 3.87\ \mu_B$. Thus both the calculated Curie constant and the effective magnetic moment are smaller than the measured values. This is expected, as previous measurements of Co^{2+} ions in the high spin state, have had effective moments between 4.3 – 5 μ_B, which is where the measured effective moment for our sample lies. This is because the orbital angular moment is assumed to be "quenched" within these systems, but there could be a small contribution, so an increase in the effective magnetic moment.

Conclusions

The coordination complex $[(N_2H_5)_2Co(HPO_4)_2]$ was synthesized by slow evaporation method. Its crystal structure consists of CoN_2O_4 and $PO_3(OH)$ alternating units connected through their vertices in 4-membered rings, which are further linked via their corners in an infinite one-dimensional (1D) chain running along [100]. The 3D framework resulting from the stacking of parallel chains is stabilized via hydrogen bond interactions between the hydrazine ligands and phosphate O atoms. The IR spectrum showed the expected bands of hydrazine

and phosphate anion. The thermogravimetric analysis shows that the dehydrogenation of phosphate takes place in one step consisting mainly of the loss of hydrazine moieties and water molecules coming from dehydration of phosphate groups and leading to the formation of cobalt phosphate. The cobalt phosphate complex exhibits a promising catalytic activity in the oxidation and decomposition of methylene blue (MB) dye with hydrogen peroxide under ambient conditions only for 2 hours. The ac magnetic susceptibility shows a peak indicating antiferromagnetic order, with a Neel temperature of 5.5 K. Above 50 K, the fit of the Curie-Weiss equation to the ac magnetic susceptibility gives an average Curie-Weiss constant of -11.8 K.

Acknowledgements

This research was supported by CNRST (Morocco) (URAC 19). The crystallographic part was supported by the project 18-10438S of the Czech Science Foundation using instruments of the ASTRA laboratory established within the Operation program Prague Competitiveness - project CZ.2.16/3.1.00/24510. Authors would thank Prof. M. EZAHRI (Laboratoire Matériaux et Environnement, Faculté des Sciences, Université Ibn Zohr, Agadir) for the IR measurements.

Figures and Tables Caption

Figure 1: Unit cell in the crystal structure of $[(N_2H_5)_2Co(HPO_4)_2]$.

Figure 2: Coordination of Co in the framework of $[(N_2H_5)_2Co(HPO_4)_2]$ (thermal ellipsoids are shown at 50% probability).

Figure 3: The [010]-parallel chain of $[(N_2H_5)_2Co(HPO_4)_2]$ molecules.

Figure 4: Projection along [100] of the crystal structure of $[(N_2H_5)_2Co(HPO_4)_2]$ emphasizing the hydrogen bonding (dashed lines) between the chains.

Figure 5. Simulated (red) and experimental (black) powder X-ray diffraction patterns of $[(N_2H_5)_2Co(HPO_4)_2]$.

Figure 6. FTIR spectrum of $[(N_2H_5)_2Co(HPO_4)_2]$.

Figure 7. TG-DTA curves of $[(N_2H_5)_2Co(HPO_4)_2]$ complex.

Figure 8 : FTIR spectrum of $[(N_2H_5)_2Co(HPO_4)_2]$ after treatment at 600°C.

Figure 9: The change of methylene blue concentration as a function of time after adding the cobalt phosphate complex.

Figure 10: Magnetisation as a function of temperature, for zero-field cooled (blue) and field-cooled (red), with applied field of 100 Oe. Inset: Magnetisation as a function of magnetic field, for 2.5 K (black), 5 K (blue) and 300 K (red).

Figure 11: AC susceptibility (χ') as a function of temperature, at 10 Hz (blue), 100 Hz (red) and 1000 Hz (black). Inset: Zoom in on the low temperature AC susceptibility (χ') data.

Figure 12: Susceptibility*temperature ($\chi'T$) as a function of temperature for 10 Hz (blue circles), 100 Hz (red squares) and 1000 Hz (black triangles). The solid black line is the Curie-Weiss law fitted to the data. Inset: AC susceptibility (χ'') as a function of temperature for 1000 Hz.

Table 1: Experimental data collections details for $[(N_2H_5)_2Co(HPO_4)_2]$.

Table 2: Fractional atomic coordinates and isotropic or equivalent isotropic displacement parameters ($Å^2$).

Table 3: Selected bond lengths and angles (Å, °) for $[(N_2H_5)_2Co(HPO_4)_2]$.

Table 4: Hydrogen-bond geometry (Å, °) for $[(N_2H_5)_2Co(HPO_4)_2]$.

References

[1] A. K. Cheetham, G.Férey, T. Loiseau. *Angew. Chem. Int. Ed. Engl.,* **38**, 3268 (1999).

[2] Y-C. Jiang, S. L. Wang, K. H. Li, N. Nguyen, A. Ducouret. *Chem. mat.*, **15**, 1633 (2003).

[3] S. Natarajan, S. Neeraj, A. Choudhury, C. N. R. Rao. *Inorg. Chem*., **39**, 1426 (2000).

[4] C. N. R. Rao, S. Natarajan, S. Neeraj. *J. Am. Chem. Soc.*, **122**, 2810 (2000).

[5] A.M. Chippindale, F.O. Gaslain, A.R. Cowley, A.V. Powell. *J. Mat. Chem.*, **11**, 3172 (2001).

[6] R. H. Jones, J. M. Thomas, R. Xu, Q. Huo, Y. Xu, A. K. Cheetham, D. Bieber, *J. Chem. Soc., Chem. Commun.*, **17**, 1170 (1990).

[7] Q. Gao, J. Chen, S. Li, R. Xu, J. M. Thomas, M. Light, M. B. Hursthouse., *J. Solid State Chem.*, **127**, 145 (1996).

[8] I. D. Williams, J.Yu, J., Gao, Q., Chen, J. and Xu, R. *Chem. Commun*, **14**, 1273 (1997).

[9] A. M. Chippindale, C. Turner. *J. Solid State Chem.*, **128**, 318 (1997).

[10] T. Loiseau, F. Serpaggi, G. Férey. *Chem. Commun.*, **12**, 1093 (1997).

[11] A. M. Chippindale, A. D. Bond, A. D. Law, A. R. Cowley. *J. Solid State Chem.*, **136**, 227 (1998).

[**12**] B. El Bali, R. Essehli, F. Capitelli, M. Lachkar. *Acta Cryst.*, **E61**, i52 (2005).

[13] M. Touaiher, M. Bettach, K. Benkhouja, M. Zahir, M. A. G. Aranda, S. Bruque. *Ann Chim Sc-Mat*., **26**, 49 (2001).

[14] I. Messouri, B. El Bali, F. Capitelli, J.F. Piniella, M. Lachkar, Z. Slimani. *Acta Cryst.*, **E61**, i129 (2005).

[15] R. Essehli, M. Lachkar, I. Svoboda, H. Fuess, B. El Bali. *Acta Cryst.,* **E61**, i64 (2005).

[16] R. Essehli, M. Lachkar, I. Svoboda, H. Fuess, B. El Bali. *Acta Cryst.*, **E61**, i32 (2005).

[17] (a) M. Fujita, Y. J. Kwon, S. Washizu, K. Ogura. *J. Am. Chem. Soc.*, **116**, 1151(1994); (b) R. W. Gable, B. F. Hoskins, R. Robson, *J. Chem. Soc., Chem. Commun.*, 1677 (1990).

[18] O. Khan, Y. Pei, M. Verdaguer, J. P. Renard, J. Sletten, *J. Am. Chem. Soc*., **110**, 782 (1988).

[19] H. Oudghiri-Hassani. *J. Mater. Environ. Sci*., **9**, 1051 (2018).

[20] Agilent (2010). CrysAlis PRO. Agilent Technologies, Yarnton, England.

[21] (a) SIR97: A. Altomare, M.C. Burla, M. Camalli, G.L. Cascarano, C. Giacovazzo, A. Guagliardi, A.G.G. Moliterni, G. Polidori G, R. Spagna. *J. Appl. Cryst.*, **32**, 115 (1999). (b) SUPERFLIP, L. Palatinus L, G. Chapuis. *J. Appl. Cryst*, **40**, 786 (2007).

[22] V. Petříček, M. Dušek, L. Palatinus, L. *Z. Kristallogr*., **229**, 345 (2014).

[23] K. Brandenburg K, H. Putz. *Crystal Impact GbR*, Postfach 1251, D 53002 Bonn, (2005) Germany.

[24] R. Ouarsal, B. El Bali, M. Lachkar, M. Dusek, K. Fejfarova. *Acta Cryst.*, **E61**, i168 (2005).

[25] W. K. Chang, R. K. Chiang, S. L. Wang. *J. Solid State Chem.*, **180**, 1713 (2007).

[26] K. Robinson, GV. Gibbs, PH. Ribbe. *Science.,*172, 567 (1971).

[27] M.E. Fleet. *Miner. Mag.,* **40**, 531 (1976).

[28] F. A. I. Ngopoh, M. Lachkar, T. Đorđević, C.L. Lengauer, B. El Bali. *J. Chem. Crystallogr.*, **45**, 369 (2015).

[29] G. Socrates, Infrared and Raman characteristic group frequencies: tables and charts. John Wiley & Sons (2004).

[30] D. Gajapathy, S. Govindarajan, K. C. Patil, H. Manohar. *Polyhedron*, ***2***(**9**), 865 (1983).

[31] K. C. Patil, T. M. Rattan, (Eds.). John Wiley & Sons (2014).

[32] M. Daturi, A. Guesdon, M. M. Borel. *J. Mat. Chem.*, **11**, 1726 (2001).

[33] G. Herzberg. Infrared and Raman Spectra of Polyatomic Molecules. Ninth ed., **2**, D. *Van Nostrand Company*, Inc., Princeton, 1945.

[34] K. Nakamoto. Infrared and Raman Spectra of Inorganic and Coordination Compounds. *Wiley*, New York, 1997.

[35] I. A. Salem, M. S. El-Maazawi, *Chemosphere*, *41*(8), 1173(2000).

[36] AH. Morrish. The physical principles of magnetism. IEEE, New York (2001).

[37] B. C. Melot, G. Rousse, J. N.Chotard, M. C. Kemei, J. Rodríguez-Carvajal, J.M. Tarascon. *Phys. Rev*., **23**, 2922(2011).

[38] B. C. Melot, J.N. Chotard, G. Rousse, M. Ati, M. Reynaud, J.M. Tarascon. *Inorg. Chem.*, **50**, 7662(2011).

[39] A. S. Borovik-Romanov, V. R. Karasik, N. M. Kreines. *J. Exptl. Theoret. Phys.,***4**, 18(1957).

Table 1: Experimental data collections details for $[(N_2H_5)_2Co(HPO_4)_2]$.

Crystal data	
Chemical formula	$CoH_{12}N_4O_8P_2$
Formula weight Mr(g/mol); *F*(000)	316.79; 322
Crystal system, S.G	Monoclinic, $P2_1/c$
a, b, c (Å) ; β (°)	5.3665(3), 11.1271(6), 7.7017 (4) ; 104.843(4)
V (Å3) ; Z	444.55 (4) ; 2
Crystal size (mm); □ (mm^{-1})	0.46 × 0.21 × 0.18; 2.33
Data collection	
Diffractometer	Xcalibur, AtlasS2, Gemini ultra
Absorption correction	Analytical from crystal shape combined with spherical harmonics *CrysAlis PRO* 1.171.39.9g (Rigaku Oxford Diffraction, 2015)
*T*min, *T*max	0.502, 0.703
No. of measured, independent and observed [I > 3σ(I)] reflections	6460, 1164, 1089
*R*int	0.018
Refinement	
R[*F*2 >3σ(*F*2)], *wR*(*F*2), S	0.019, 0.070, 1.77 [a]
No. of reflections	1164
No. of parameters	80
No. of restraints	5
H-atom treatment	H atoms treated by a mixture of independent and constrained refinement
Δρmax, Δρmin (e $Å^{-3}$)	0.27, -0.27

[a] JANA2006 does not refine the weighting scheme. Therefore, the goodness of fit is usually fairly above 1, especially for well-exposed data bearing information about bonding electrons.

Table 2: fractional atomic coordinates and isotropic or equivalent isotropic displacement parameters ($Å^2$)

	x	*y*	*z*	*U*iso*/*U*eq
Co1	0	0	0	0.00923 (12)
P1	0.60215 (7)	−0.04778 (4)	0.26355 (5)	0.00936 (13)
O1	0.64645 (19)	−0.12978 (11)	0.43920 (16)	0.0151 (3)

O2	−0.17371 (19)	−0.07833 (10)	0.18625 (16)	0.0138 (3)
O3	0.34337 (18)	−0.08322 (10)	0.14178 (15)	0.0145 (3)
O4	0.6047 (2)	0.08400 (10)	0.32536 (16)	0.0148 (3)
N5	0.0739 (2)	0.16063 (13)	0.15688 (19)	0.0137 (4)
N6	−0.1505 (2)	0.23451 (12)	0.1462 (2)	0.0167 (4)
H1n6	−0.102117	0.307025	0.181772	0.0201*
H2n6	−0.243646	0.236625	0.035696	0.0201*
H3n6	−0.240894	0.204448	0.21469	0.0201*
H1n5	0.191 (3)	0.2007 (15)	0.121 (3)	0.0164*
H2n5	0.136 (3)	0.1466 (19)	0.2710 (6)	0.0164*
H1o1	0.547 (3)	−0.1104 (19)	0.506 (2)	0.0181*

Table 3: Bond distances and angles (Å, º) for $[(N_2H_5)_2Co(HPO_4)_2]$

Co1—O2	2.0903 (15)	O1—H1o1	0.860 (18)
Co1—O2^{i}	2.0903 (15)	N5—N6	1.4430 (16)
Co1—O3	2.1011 (11)	N5—H1n5	0.873 (18)
Co1—O3^{i}	2.1011 (11)	N5—H2n5	0.870 (6)
P1—O2^{ii}	1.5114 (14)	N6—H1n6	0.8702
P1—O3	1.5151 (11)	N6—H2n6	0.8699
P1—O4	1.5407 (13)	N6—H3n6	0.8698
O2—Co1—O2^{i}	180.0 (5)	Co1—O3—P1	138.57 (7)
O2—Co1—O3	86.88 (5)	N6—N5—H1n5	110.3 (9)
O2—Co1—O3^{i}	93.12 (5)	N6—N5—H2n5	104.8 (12)
O2^{i}—Co1—O3	93.12 (5)	H1n5—N5—H2n5	106.8 (17)
O2^{i}—Co1—O3^{i}	86.88 (5)	N5—N6—H1n6	109.46
O3—Co1—O3^{i}	180.0 (5)	N5—N6—H2n6	109.47
O2^{ii}—P1—O3	113.17 (8)	N5—N6—H3n6	109.46

O2^{ii}—P1—O4	113.00 (7)	H1n6—N6—H2n6	109.46
O3—P1—O4	111.90 (6)	H1n6—N6—H3n6	109.47
Co1—O2—P1^{iii}	135.77 (7)	H2n6—N6—H3n6	109.5

Symmetry codes: (i) -*x*, -*y*, -*z*; (ii) *x*+1, *y*, *z*; (iii) *x*-1, *y*, *z*.

Table 4 : Hydrogen-bond geometry (Å, º) for $[(N_2H_5)_2Co(HPO_4)_2]$

D—H···*A*	*D*—H	H···*A*	*D*···*A*	*D*—H···*A*
N6—H1*n*6···O2^{iv}	0.87	2.02	2.8074 (16)	149.90
N6—H3*n*6···O4^{iii}	0.87	1.89	2.7137 (19)	157.42
N5—H1*n*5···O1^{v}	0.873 (18)	2.174 (14)	2.9678 (17)	150.9 (13)
N5—H2*n*5···O1^{vi}	0.870 (6)	2.246 (6)	3.107 (2)	170.4 (16)
O1—H1*o*1···O4^{vi}	0.860 (18)	1.725 (18)	2.572 (2)	168.2 (15)

Symmetry codes: (iii) *x*-1, *y*, *z*; (iv) -*x*, *y*+1/2, -*z*+1/2; (v) -*x*+1, *y*+1/2, -*z*+1/2; (vi) -*x*+1, -*y*, -*z*+1.

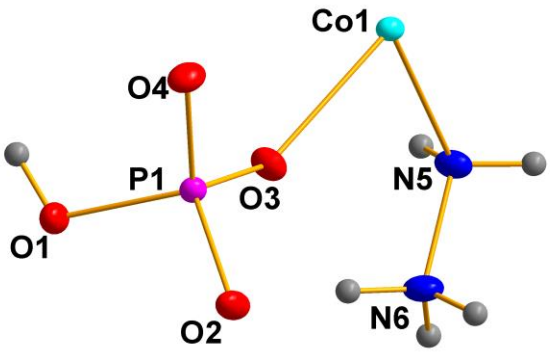
Co1
O4
P1
O3
N5
O1
O2
N6

Figure 1

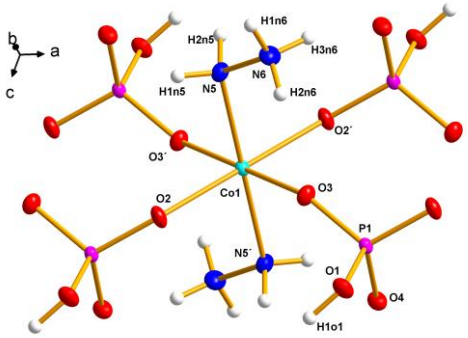
b
a
c
H2n5
H1n6
H3n6
N6
H1n5
N5
H2n6
O2'
O3'
Co1
O3
O2
P1
N5'
O1
O4
H1o1

Figure 2

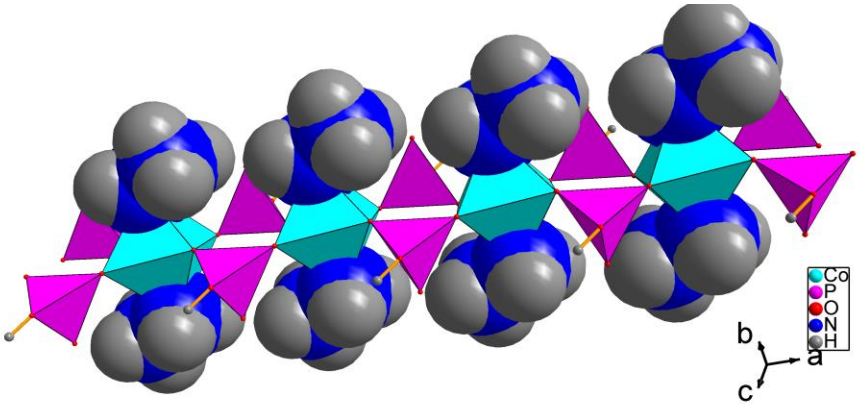

Figure 3

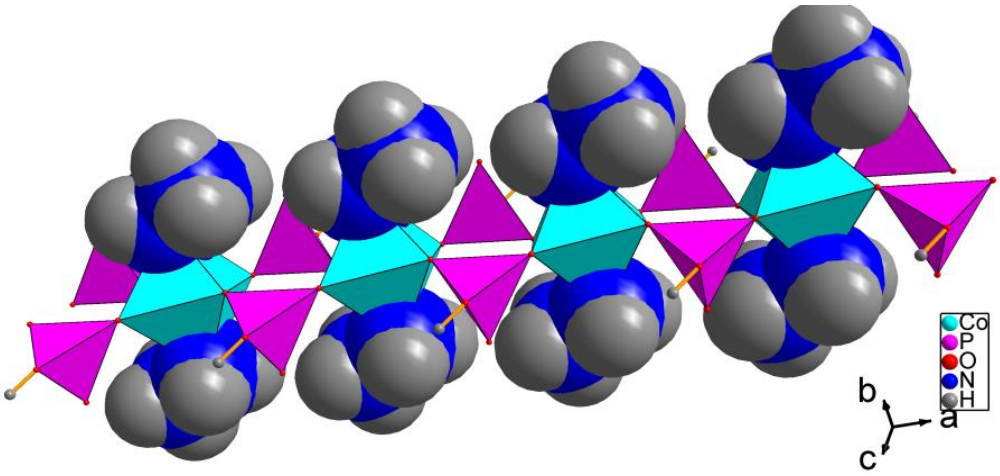

Figure 4

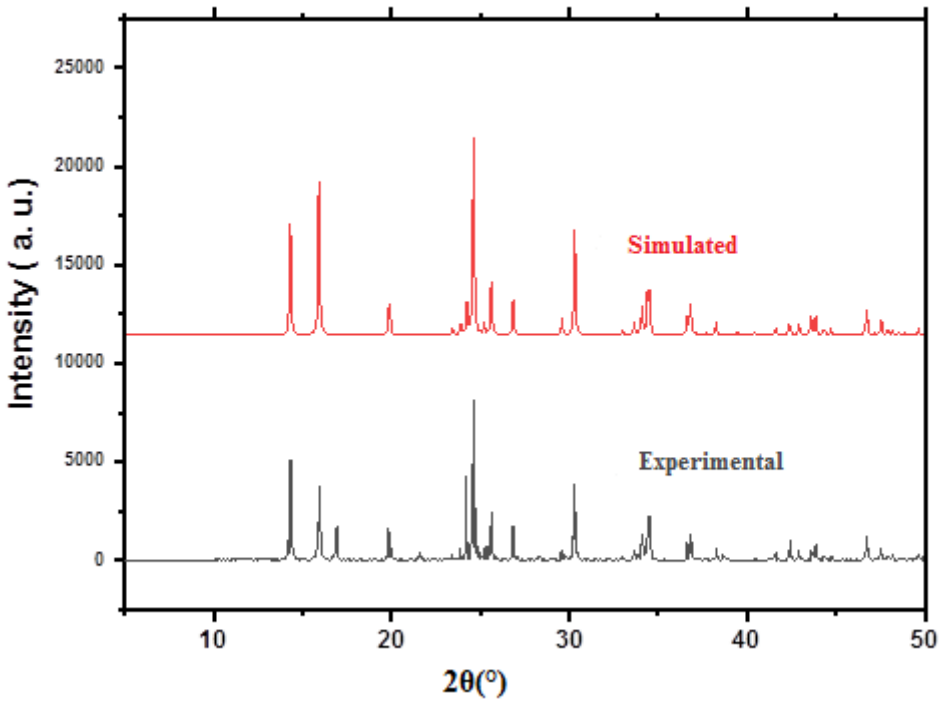

Figure 5

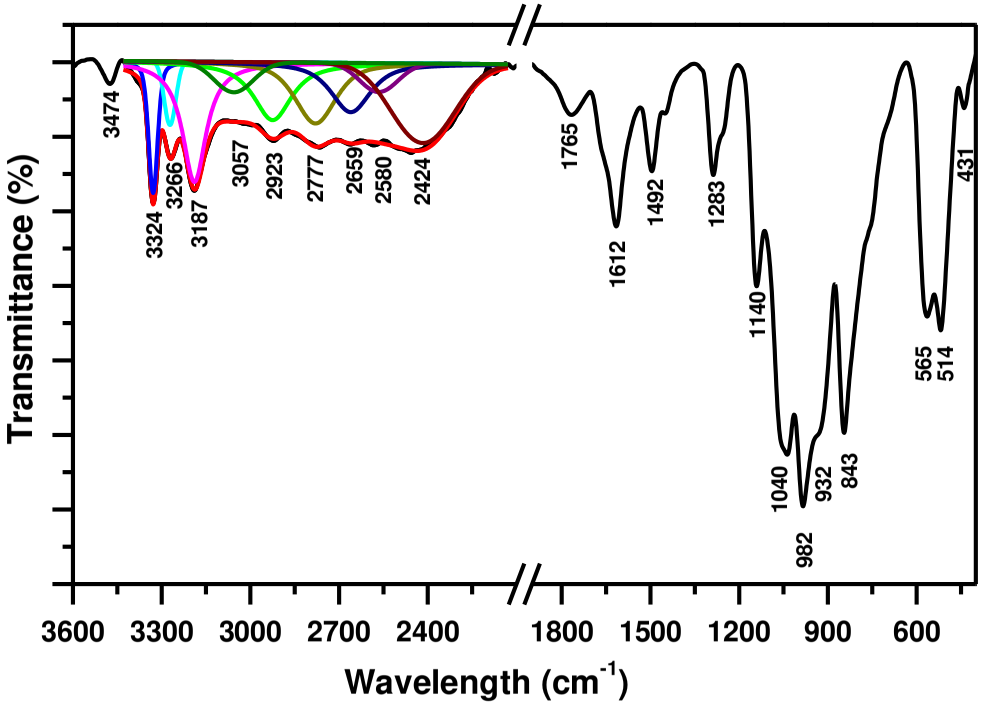
Transmittance (%)
3474
3324
3266
3187
3057
2923
2777
2659
2580
2424
1765
1612
1492
1283
1140
1040
982
932
843
565
514
431
3600
3300
3000
2700
2400
1800
1500
1200
900
600
Wavelength (cm-1)

Figure 6

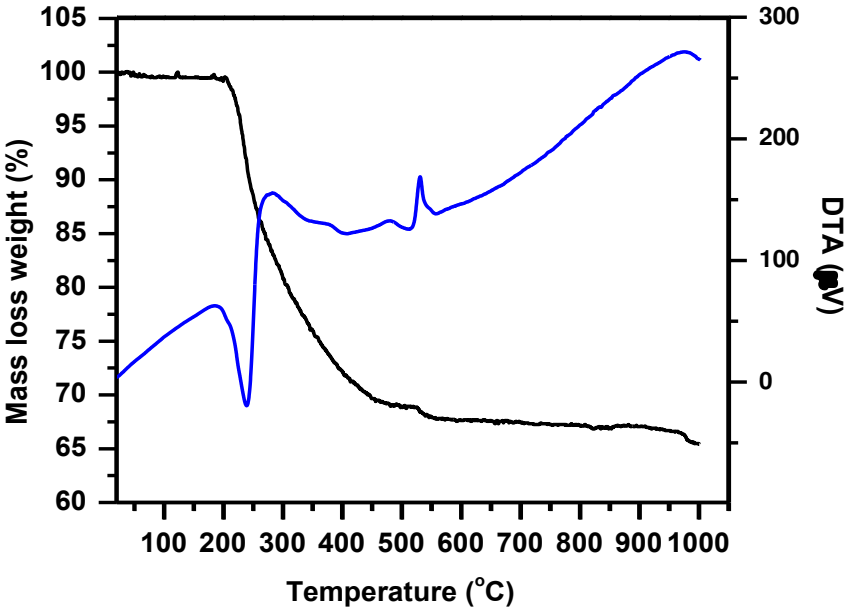
105
100
95
90
85
80
75
70
65
60
Mass loss weight (%)
300
200
100
0
DTA (μV)
100 200 300 400 500 600 700 800 900 1000
Temperature (°C)

Figure 7

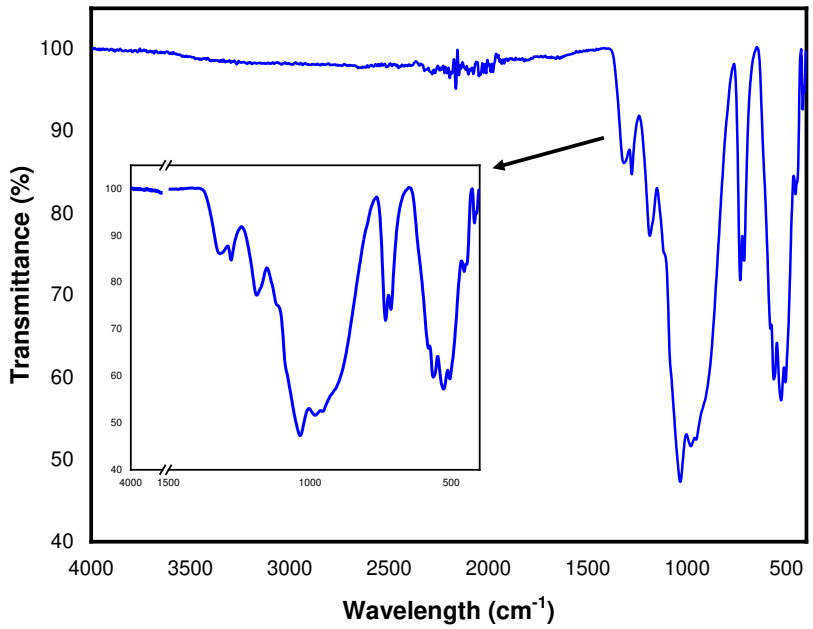
Transmittance (%)
100
90
80
70
60
50
40
4000
3500
3000
2500
2000
1500
1000
500
Wavelength (cm-1)
100
90
80
70
60
50
40
4000
1500
1000
500

Figure 8

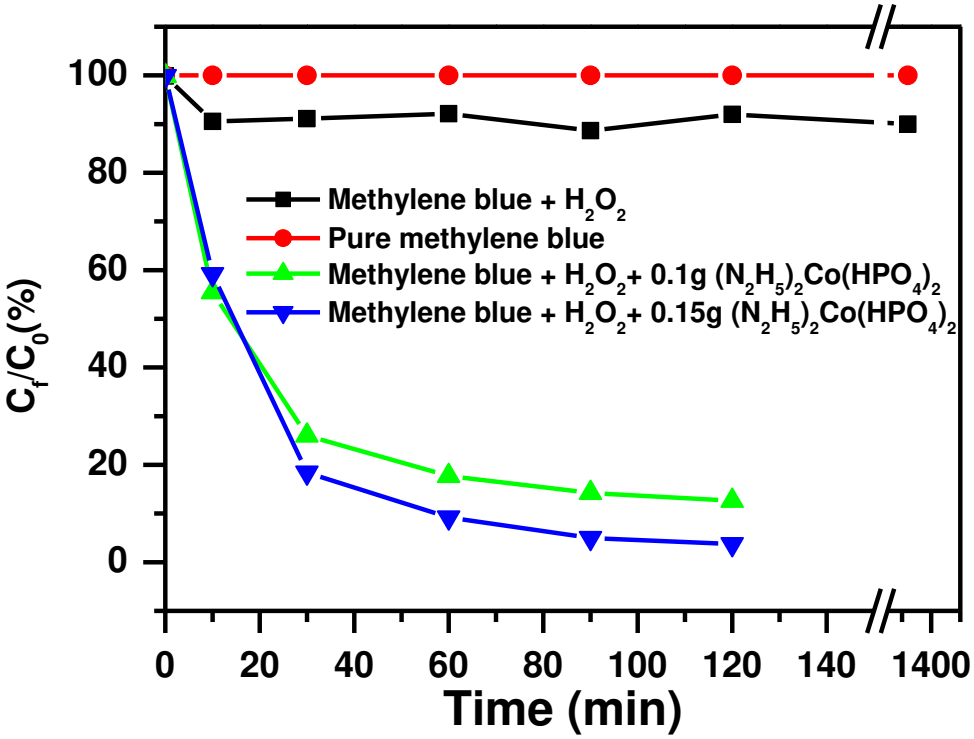
100
80
60
40
20
0
C_f/C_0(%)
0
20
40
60
80
100
120
140
1400
Time (min)
Methylene blue + H_2O_2
Pure methylene blue
Methylene blue + H_2O_2+ 0.1g $(N_2H_5)_2Co(HPO_4)_2$
Methylene blue + H_2O_2+ 0.15g $(N_2H_5)_2Co(HPO_4)_2$

Figure 9

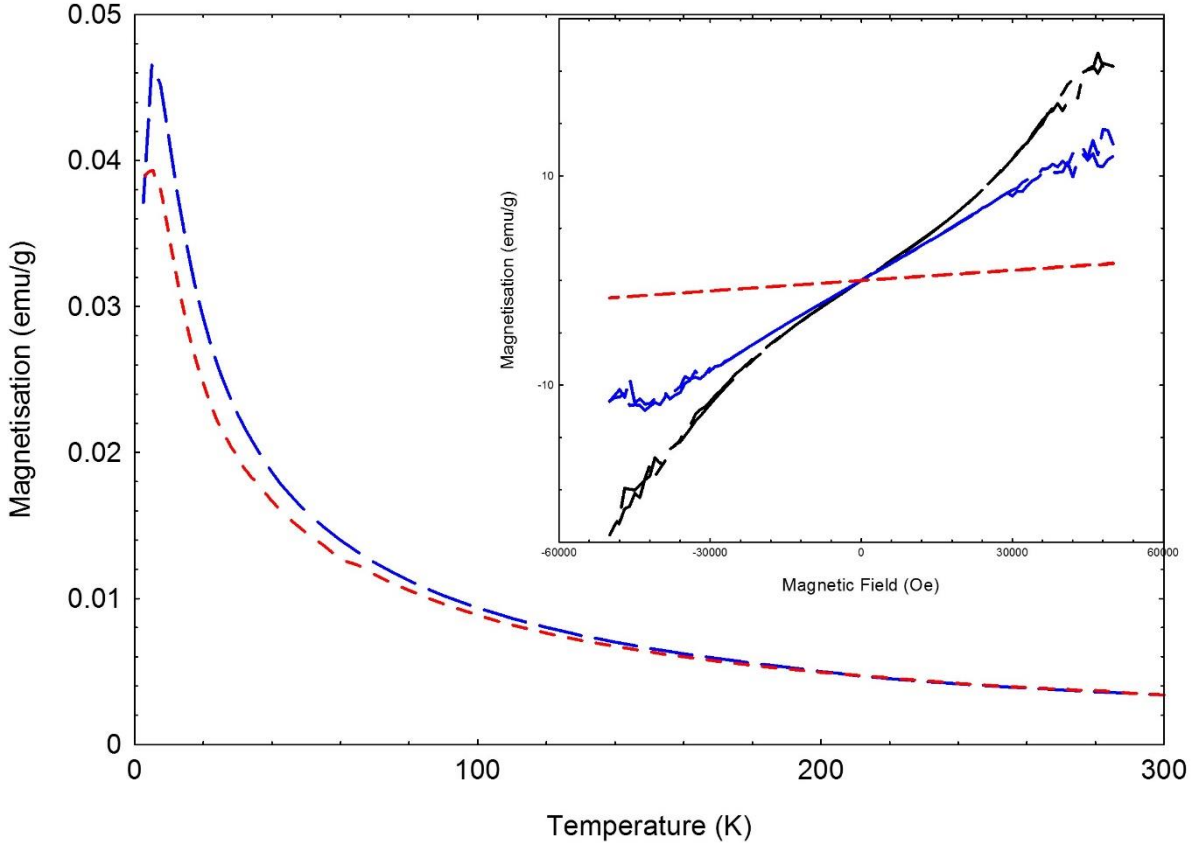
0.05
0.04
0.03
0.02
0.01
0
Magnetisation (emu/g)
0
100
200
300
Temperature (K)
10
-10
Magnetisation (emu/g)
-60000
-30000
0
30000
60000
Magnetic Field (Oe)

Figure 10

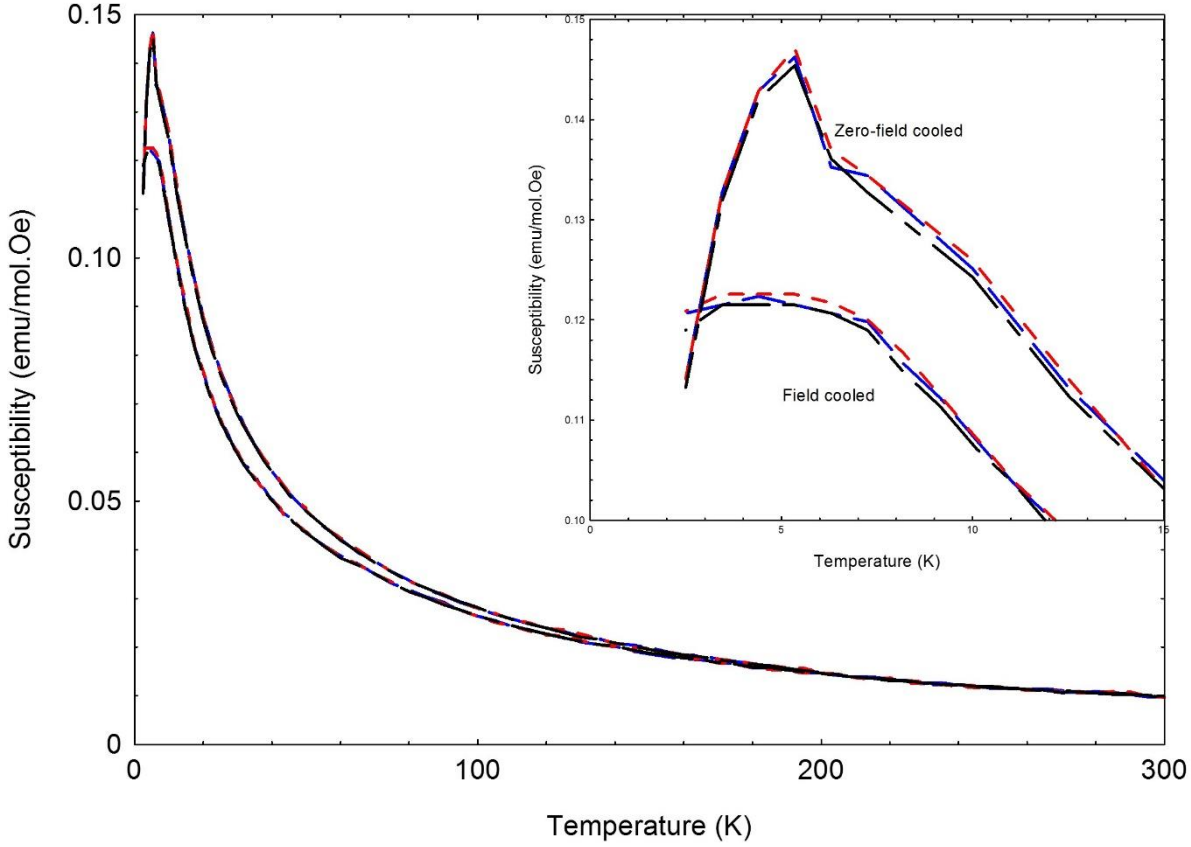
Susceptibility (emu/mol.Oe)
Temperature (K)
0.15
0.10
0.05
0
0
100
200
300
Zero-field cooled
Field cooled
Susceptibility (emu/mol.Oe)
Temperature (K)
0.15
0.14
0.13
0.12
0.11
0.10
0
5
10
15

Figure 11

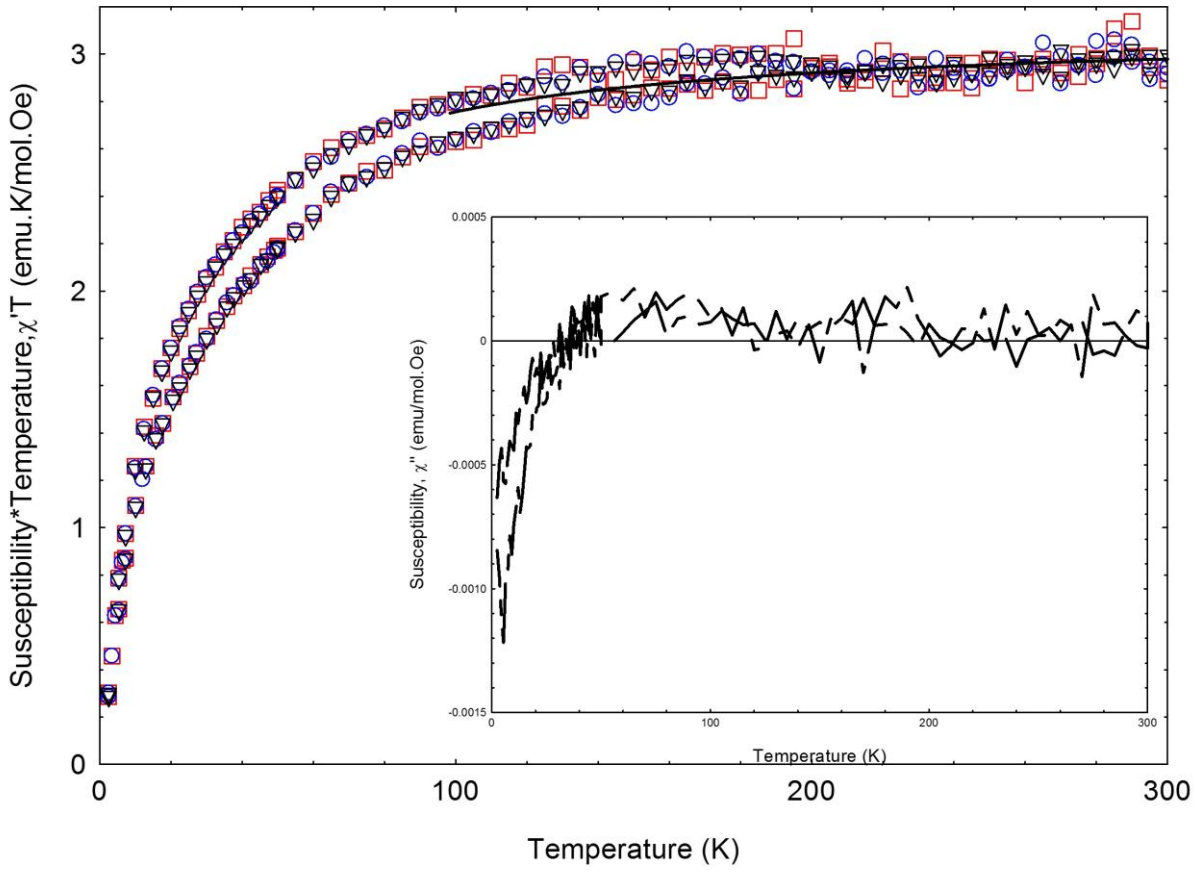
Susceptibility*Temperature,χ'T (emu.K/mol.Oe)
Temperature (K)
0
1
2
3
0
100
200
300
Susceptibility, χ'' (emu/mol.Oe)
0.0005
0
-0.0005
-0.0010
-0.0015
0
100
200
300
Temperature (K)

Figure 12